Moiré volume Bragg grating filter with tunable bandwidth

Sergiy Mokhov,* Daniel Ott, Ivan Divliansky, Boris Zeldovich and Leonid Glebov

CREOL − the College of Optics and Photonics, University of Central Florida, Orlando, FL 32816, USA
*smokhov@creol.ucf.edu

Abstract: We propose a monolithic large-aperture narrowband optical filter based on a moiré volume Bragg grating formed by two sequentially recorded gratings with slightly different resonant wavelengths. Such recording creates a spatial modulation of refractive index with a slowly varying sinusoidal envelope. By cutting a specimen at a small angle, to a thickness of one-period of this envelope, the longitudinal envelope profile will shift from a sine profile to a cosine profile across the face of the device. The transmission peak of the filter has a tunable bandwidth while remaining at a fixed resonant wavelength by a transversal shift of incidence position. Analytical expressions for the tunable bandwidth of such a filter are calculated and experimental data from a filter operating at 1064 nm with bandwidth range 30-90 pm is demonstrated.

OCIS codes: (090.2890) Holographic optical elements; (300.6320) Spectroscopy, high-resolution.

References and links

1. C. Fricke-Begemann, M. Alpers, and J. Höffner, "Daylight rejection with a new receiver for potassium resonance temperature lidars," Opt. Lett. **27**(21), 1932–1934 (2002).
2. G. A. Rakuljic and V. Leyva, "Volume holographic narrow-band optical filter," Opt. Lett. **18**(6), 459–61 (1993).
3. Y. Akahane, T. Asano, H. Takano, B.-S. Song, Y. Takana, and S. Noda, "Two-dimensional photonic-crystal-slab channel-drop filter with flat-top response," Opt. Express **13**(7), 2512–2530 (2005).
4. Z. Cheng, D. Liu, Y. Yang, L. Yang, and H. Huang, "Interferometric filters for spectral discrimination in high-spectral-resolution lidar: performance comparisons between Fabry-Perot interferometer and field-widened Michelson interferometer," Appl. Opt. **52**(32), 7838–7850 (2013).
5. J. Bland-Hawthorn, W. van Breugel, P. R. Gillingham, I. K. Baldry, and D. H. Jones, "A Tunable Lyot Filter at Prime Focus: a Method for Tracing Supercluster Scales at z ~ 1," Astrophys. J. **563**(2), 611–628 (2001).
6. G. B. Venus, A. Sevian, V. Smirnov, and L. B. Glebov, "High-brightness narrow-line laser diode source with volume Bragg-grating feedback," Proc. SPIE **5711**, 166–176 (2005).
7. L. Glebov, J. Lumeau, S. Mokhov, V. Smirnov, and B. Zeldovich, "Reflection of light by composite volume holograms: Fresnel corrections and Fabry-Perot spectral filtering," J. Opt. Soc. Am. A **25**(3), 751–764 (2008).
8. S. Legoubin, E. Fertein, M. Douay, P. Bernage, P. Niay, F. Bayon, and T. Georges, "Formation of moiré grating in core of germanosilicate fibre by transverse holographic double exposure method," Electron. Lett. **27**(21), 1945–1947, (1991).
9. R. J. Campbell and R. Kashyap, "Spectral profile and multiplexing of Bragg gratings in photosensitive fiber," Opt. Lett. **16**(12), 898–900 (1991).
10. L. A. Everall, K. Sugden, J. A. R. Williams, I. Bennion, X. Liu, J. S. Aitchison, S. Thoms, and R. M. De La Rue, "Fabrication of multipassband moiré resonators in fibers by the dual-phase-mask exposure method," Opt. Lett. **22**(19), 1473–1475 (1997).
11. R. Kashyap, *Fiber Bragg Gratings*, 2nd ed. (Academic, 2009).
12. V. Smirnov, J. Lumeau, S. Mokhov, B. Zeldovich, and L. Glebov, "Ultranarrow bandwidth moiré reflecting Bragg gratings recorded in photo-thermo-refractive glass," Opt. Lett. **35**(4), 592–594 (2010).
13. A. Sevian, O. Andrusyak, I. Ciapurin, V. Smirnov, G. Venus, and L. Glebov, "Efficient power scaling of laser radiation by spectral beam combining," Opt. Lett. **33**(4), 384–386 (2008).
14. H. Kogelnik, "Coupled wave theory for thick hologram gratings," Bell Syst. Tech. J. **48**(9), 2909–2945 (1969).
15. V. Mizrahi and J. E. Sipe, "Optical properties of photosensitive fiber phase gratings," J. Lightwave Technol. **11**(10), 1513–1517 (1993).

#212248 - $15.00 USD Received 16 May 2014; revised 25 Jul 2014; accepted 28 Jul 2014; published 15 Aug 2014

16. L. Glebov, "Volume Holographic Elements in a Photo-Thermo-Refractive Glass," J. Holography and Speckle **5**(1), 77–84 (2009).
17. E. Hecht, *Optics*, 4th ed. (Addison-Wesley, 2001), Chap. 9.6 Multiple Beam Interference.
18. I. Divliansky, D. Ott, B. Anderson, D. Drachenberg, V. Rotar, G. Venus and L. Glebov, "Multiplexed volume Bragg gratings for spectral beam combining of high power fiber lasers," Proc. SPIE **8237**, 823705 (2012).
19. M. SeGall, D. Ott, I. Divliansky, and L. B. Glebov, "Effect of aberrations in a holographic system on reflecting volume Bragg gratings," Appl. Opt. **52**(32), 7826–7831 (2013).

1. Introduction

The ability to isolate information encoded in some spectral band of a light signal is critical to a number of sensing and communication technologies and there exists an abundance of optical filters to fulfill these roles [1–5]. In the pursuit of improved performance for these applications, for example higher spectral resolution for lidar or for improving the number of WDM channels, filters with narrow bandwidths and high efficiency are desirable. In addition, the creation of narrowband, highly coherent light sources which serve as sources for many of these same applications depend on similar filtering technology, be it inherent to the design or an external component. As an example, spectral narrowing of laser diode emission can be achieved using a spectrally selective mirror [6]. This example utilizes a uniform reflective volume Bragg grating (VBG) recorded in photo-thermo-refractive (PTR) glass to produce narrowband, low loss, high efficiency spectral filtering. Such filters are most directly comparable to fiber Bragg gratings (FBGs) but have the advantage of a large aperture, which allows free space operation with high power laser beams. Typically a PTR VBG has a full width at half maximum (FWHM) reflection bandwidth in the range of 50-500 pm. The bandwidth depends on the amplitude of refractive index modulation (RIM) and the thickness. To achieve narrower bandwidth filtering, a resonant Fabry-Perot cavity can be formed with two VBGs with mutual phase π-shift between their profiles of spatial RIMs. If no phase shift is introduced, the whole compound device works as if it were a single VBG with double thickness.

Such a compound VBG cavity was demonstrated in [7] but it was not robust. However, a monolithic filter with similar characteristics can be fabricated based on the moiré effect by superimposing two gratings with slightly different periods within the same volume. In case of the two grating wavevectors being in the same direction, the total recorded pattern has a carrier spatial frequency equal to the average frequency of two gratings, while the amplitude envelope varies slowly with a spatial frequency equal to half of the difference of the two individual frequencies, namely

$$\cos(Q_1 z) + \cos(Q_2 z) = 2\cos(Qz)\cos(qz), \quad Q = \tfrac{1}{2}(Q_1 + Q_2), \quad q = \tfrac{1}{2}(Q_1 - Q_2), \tag{1}$$

Two neighbor semi-periods of length $l = \pi/q$, separated by a zero point of the slowly varying envelope $\cos(qz)$, have a mutual phase shift of π between their Bragg modulations. This slow periodic variation of refractive index modulation has been implemented in FBGs [8], and properties of moiré FBGs were intensively studied [9–11]. A volume monolithic device based on moiré pattern was demonstrated in PTR glass [12] but no comprehensive theoretical analysis was provided at that time and no potential capabilities of such elements were studied. In this paper we will discuss features of one-dimensional theory of moiré Bragg gratings and will present results of experimental implementation of a moiré resonant VBG cavity with a narrow tunable bandwidth.

2. Notations and basic equations

Consider two uniform gratings with equal amplitudes of RIM $N_1/2$ and slightly different vacuum resonant wavelengths λ_1 and λ_2 and mutually aligned wave vectors along the z-axis which have been recorded in the same medium with background refractive index n_0. The resulting modulated refractive index is

#212248 - $15.00 USD Received 16 May 2014; revised 25 Jul 2014; accepted 28 Jul 2014; published 15 Aug 2014

$$n(z) = n_0 + n_{1,\varphi}(z)\cos(Qz+\gamma), \quad Q = 4\pi n_0/\lambda_0, \quad \lambda_0 = \tfrac{1}{2}(\lambda_1+\lambda_2),$$
$$n_{1,\varphi}(z) = N_1 \sin(\pi z/l + \varphi), \quad l = \lambda_0^2/(2n_0\Delta\lambda), \quad \Delta\lambda = \lambda_2 - \lambda_1, \tag{2}$$

were λ_0 is vacuum Bragg resonant wavelength of the moiré grating, $n_{1,\varphi}(z)$ is the slowly varying envelope of the moiré pattern with amplitude N_1 and spatial semi-period l, phase γ defines the position of the fast spatial modulation of refractive index and phase φ defines the position of the slow varying envelope on the z-axis as shown in Fig. 1(a).

Let us analyze the spectral properties of such a resonator. Propagation of monochromatic electromagnetic plane waves inside the reflective VBG may be formulated in terms of counter-propagating waves $A(z)\exp(-i\omega t+ikz)$ and $B(z)\exp(-i\omega t-ikz)$ with $k = n_0\omega/c = 2\pi n_0/\lambda$ [7]. The slowly varying envelopes $A(z)$ and $B(z)$ are coupled by equations

$$\begin{cases} \frac{d}{dz}A = i\kappa(z)Be^{-2iDz+i\gamma}, \\ \frac{d}{dz}B = -i\kappa(z)Ae^{2iDz-i\gamma}, \end{cases} \quad \kappa(z) = \pi n_{1,\varphi}(z)/\lambda_0, \quad D = k - \tfrac{1}{2}Q, \quad k = 2\pi n_0/\lambda, \tag{3}$$

where $\kappa(z)$ is the coupling parameter with $n_{1,\varphi}(z)$ from Eq. (2) and D is a z-independent parameter of detuning from the Bragg resonance condition which corresponds to $D = 0$.

At skew propagation with the angle θ_{in} inside the VBG, see [7], the coupling parameter should be divided by $\cos\theta_{in}$ and, in the case of TM polarization, multiplied by $\cos(2\theta_{in})$. Additionally k should be substituted by $k\cos\theta_{in}$ in the expression for D in Eq. (3) so the resonant wavelength will be shifted to

$$\lambda_{res} = \lambda_0 \cos\theta_{in} \approx \lambda_0(1 - \tfrac{1}{2}\theta_{air}^2/n_0^2) \tag{4}$$

where θ_{air} is the angle of incidence in air. This angular adjustment of the spectral resonant properties is often used in experimental setups with VBGs [13], a feature that is absent for FBGs. Below we discuss more sophisticated possibilities for VBGs provided by the presence of transverse degrees of freedom.

3. Spectral properties of moiré VBG filter

The solution of the system in Eq. (3) for a linear media can be represented in matrix form

$$\begin{pmatrix} A(z) \\ B(z) \end{pmatrix} = \hat{M}(z)\begin{pmatrix} A(0) \\ B(0) \end{pmatrix}, \quad \hat{M}(z) = \begin{pmatrix} M_{11}(z) & M_{12}(z) \\ M_{21}(z) & M_{22}(z) \end{pmatrix}. \tag{5}$$

The determinant of matrix $\hat{M}$ equals one, $\det\hat{M} = 1$, which will be also true even in the case of loss. In the absence of loss the matrix $\hat{M}$ related to Eq. (3) belongs to group SL(1,1), and it provides conservation of the expression $|A(z)|^2-|B(z)|^2$, proportional to the Poynting vector.

The problem of reflection of incident wave with amplitude $A(0)$ is formulated with boundary condition $B(L) = 0$ at the opposite side of element of length L. According to Eq. (5), this condition leads to the following expressions for amplitude reflection and transmission coefficients, r and t

$$r = B(0)/A(0) = -M_{21}(L)/M_{22}(L), \quad R = |r|^2 = \tanh^2 S,$$
$$t = A(L)/A(0) = 1/M_{22}(L), \quad T = |t|^2 = 1 - R = 1/\cosh^2 S. \tag{6}$$

Here R is reflectance, T is transmittance and the introduced parameter S is the "strength of reflection" which obeys the law of additivity [7]. In particular, for two elements reflecting in a constructive manner the total strength is the sum of their particular strengths. The equality of the matrix determinant to one was used to derive the expression for amplitude transmission coefficient t in Eq. (6).

#212248 - $15.00 USD Received 16 May 2014; revised 25 Jul 2014; accepted 28 Jul 2014; published 15 Aug 2014

The solution of Eq. (3) for a uniform grating with constant n_1 is given by Kogelnik's well-known analytic result [14]. Propagation of electromagnetic waves in a non-uniform VBG with all z-dependent $n_0(z)$, $n_1(z)$ and $\gamma(z)$ can be studied numerically only [15].

If the coupling $\kappa(z)$ depends on z only through the arbitrary real function $n_1(z)$ with constant γ, then the matrix $\hat{M}(z)$ for system in Eq. (3), at exact Bragg resonance $D = 0$, has the following analytic solution defining the resonant amplitude reflection coefficient r_0 according to Eq. (6)

$$\hat{M}_0(z) = \begin{pmatrix} \cosh S(z) & ie^{i\gamma} \sinh S(z) \\ -ie^{-i\gamma} \sinh S(z) & \cosh S(z) \end{pmatrix}, \quad S(z) = \pi/\lambda_0 \int_0^z n_1(z')dz', \quad r_0 = ie^{-i\gamma} \tanh S(L). \quad (7)$$

We see that gratings with envelope profiles $n_1(z)$ with zero integral values of $S(L) = 0$ over the grating thickness demonstrates zero reflection and 100% theoretical transmittance in the case of exact Bragg resonance according to Eqs. (6),(7). This zero condition exists for $n_{1,\varphi}(z)$ from Eq. (2) with $0 \le z \le L = 2l$. For the particular envelope phase of $\varphi = 0$ in Eq. (2) this result can be interpreted as perfect transmission through a Fabry-Perot filter of two identical reflective elements. Each of them is comprised of an apodized VBG from one semi-period of the moiré pattern with the following reflection strength

$$s_M = S(l) = \pi/\lambda_0 \int_0^l n_{1,\varphi=0}(z)dz = 2N_1 l/\lambda_0. \quad (8)$$

In [12] we have reported experimental results of the first such moiré VBG filter fabricated in PTR glass. During the recording process the glass sample was sequentially exposed with the stationary intensity interference patterns formed by splitting and overlapping two parts of flat-front UV beam at $\lambda_{UV} = 325$ nm. The angle 2α between two overlapping coherent UV waves defines the resonant VBG wavelength as $\lambda_0 = n_0\lambda_{UV}/\sin\alpha$, and for the discussed grating λ_0 was 1550 nm. A small change in the recording angle α for the second grating resulted in a moiré pattern with semi-period of the RIM envelope equal to $l = 3$ mm. These exposures were followed by a thermal development to produce a permanent change of refractive index in PTR glass. RIM of up to $10^{-3} \equiv 10^3$ppm can be achieved [16]. The modulation of each grating after development was around $\frac{1}{2}N_1 = 120$ ppm. The filter produced a narrow transmission peak which had a bandwidth of 50 pm with 95% maximum transmittance.

One can see that the strength integral from Eq. (7) for $n_{1,\varphi}(z)$ from Eq. (2) over one moiré period $2l$, equals zero regardless of the starting phase φ of envelope profile. Meaning that 100% theoretical peak transmission occurs at the same resonant Bragg wavelength λ_0 whether the envelope modulation amplitude profile is a sine period, a cosine one, or some intermediate profile between the two. But, the bandwidth of a transmission peak will depend on φ. One of the main goals of this paper is to find the formula for the bandwidth of a moiré filter depending on its parameters λ_0, n_0, l, N_1 and the starting phase φ of the moiré envelope.

Bandwidth tunability of the resonant peak is possible in a moiré VBG due to the presence of transverse degrees of freedom and it can be useful for some spectroscopic applications or in laser cavity design. Implementation of a filter with tunable bandwidth can be realized in the following way: while the wave vector **Q** of the fast Bragg modulation is directed along z-axis, the moiré pattern wave vector **q** can be very slightly tilted from z-axis by appropriately recording two gratings with non-collinear vectors $\mathbf{Q}_1$ and $\mathbf{Q}_2$. Then, with transverse shift along the x-direction, the moiré envelope profile inside such a specimen is changing from a sine to a cosine profile as illustrated in Fig. 1(a). Transmission peak shapes calculated numerically according to Eqs. (3),(5),(6) in the vicinity of the resonant wavelength for different transverse illumination points are presented in Fig. 1(b).

#212248 - $15.00 USD Received 16 May 2014; revised 25 Jul 2014; accepted 28 Jul 2014; published 15 Aug 2014

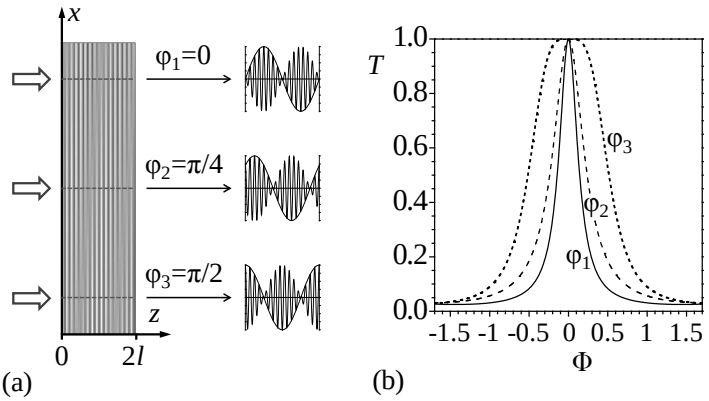

Fig. 1. (a) Scheme of a one-period moiré VBG with RIM envelope profiles of shifted phases. (b) Corresponding numerically calculated transmission peaks versus dimensionless detuning $\Phi = Dl$ for different envelope profiles.

In these simulations, the reflection strength of one semi-period in Eq. (8) was $s_M = 1.5$, and the argument of wavelength detuning is expressed through the dimensionless detuning phase $\Phi = Dl$, where the semi-period $l = L/2$ is defined in Eq. (2) and the detuning D is defined in Eq. (3).

4. Analytic theory of transmission peak bandwidths

To begin the theoretical analysis of transmission peak shapes of a resonant moiré Bragg cavity, it is instructive to start with studying more simple resonant cavities. First we will bring up the properties of a regular Fabry-Perot resonator consisting of two equivalent thin mirrors. Then we will consider resonant cavity made of two uniform Bragg gratings with mutual π phase shift between their RIMs. For all mentioned resonant cavities we will use the transfer matrix technique. By deriving the dependence of the propagation matrix element $M_{22}(L)$ on the detuning Φ in the vicinity of the transmission peak resonance we will get the spectral shape of the transmission peak as $T = 1/|M_{22}(L)|^2$ according to Eq. (6).

Suppose the reflectivity of each mirror of a regular Fabry-Perot cavity is $R = \tanh^2 s$, see Eq. (6), where strength s is a parameter of the propagation matrix $\hat{m}(s)$ through one thin mirror similar to Eq. (7). The matrix for another element shifted by distance l is similar to first matrix with additional phase matrix multipliers due to this longitudinal shift [7], so the total propagation matrix $\hat{M}$ of a two-element system is:

$$\begin{pmatrix} A \\ B \end{pmatrix}_{z=l+0} = \hat{M}\begin{pmatrix} A \\ B \end{pmatrix}_{z=-0}, \hat{M} = \hat{K}(-kl)\hat{m}(-s)\hat{K}(kl)\hat{m}(s), \ \hat{m}(s) = \begin{pmatrix} \cosh s & \sinh s \\ \sinh s & \cosh s \end{pmatrix}, \ \hat{K}(\Phi) = \begin{pmatrix} e^{i\Phi} & 0 \\ 0 & e^{-i\Phi} \end{pmatrix}. \quad (9)$$

When mirrors are attached to each other, $l = 0$, then $\hat{M}$ is the unit matrix and we have 100% resonant transmission. In general, the resonant transmission occurs at some particular wavelength λ_0 when the phase matrix in Eq. (7) is proportional to unit one $\hat{K}(k_0 l) = \pm\hat{1}$, $k_0 = 2\pi n_0/\lambda_0$, so it should be $k_0 l = \pi p$, where p is integer. We obtain the well-known result that a half-integer number of wavelengths is needed for resonant transmission: $l = p\lambda_0/(2n_0)$.

With detuning from the resonant wavelength, the transmission decreases according to a Lorentzian shape following Eqs. (9),(6):

$$\begin{aligned} &M_{22} = e^{i\Phi}(\cos\Phi - i\cosh(2s)\sin\Phi), \quad \Phi = (k-k_0)l \approx -2\pi n_0 l\delta\lambda/\lambda_0^2, \quad \delta\lambda = \lambda - \lambda_0, \\ &T = 1/|M_{22}|^2 = 1/(1+F\sin^2\Phi), \quad F = \sinh^2(2s). \end{aligned} \quad (10)$$

#212248 - $15.00 USD Received 16 May 2014; revised 25 Jul 2014; accepted 28 Jul 2014; published 15 Aug 2014

Here Φ is a phase shift in the cavity due to wavelength detuning $\delta\lambda$ and parameter F is the finesse which determines the bandwidth of the transmission peak. The standard expression for F is $4R/(1-R)^2$ [17] which coincides with ours in Eq. (10) when taking into account $R = \tanh^2 s$, see Eq. (6). The maximum reflectivity of such a resonator, given in literature as $R_{max} = 4R/(1+R)^2$, is equal $R_{max} = \tanh^2(2s)$ in our notations for a double reflection strength device consisting of two mirrors with $s = \operatorname{arctanh}\sqrt{R}$ each.

Finally, the FWHM for a high-finesse cavity, $F >> 1$, is equal to twice the wavelength detuning $\delta\lambda_{HM}$ corresponding to $\Phi_{HM} = 1/F^{1/2}$ which gives $T = 1/2$ in Eq. (10):

$$\Delta\lambda_{FWHM} = 2\left|\delta\lambda_{HM}\right| = \lambda_0^2/(\pi n_0 l)\,\Phi_{HM} = \lambda_0^2/(\pi n_0 l \sinh(2s)). \tag{11}$$

Let us now discuss uniform Bragg gratings. The propagation matrix $\hat{m}_I(s,\Phi,\gamma)$ for a grating with constant n_1 in the coupled wave system in Eq. (3) has a known analytical solution for arbitrary detuning from the resonant Bragg condition

$$\begin{pmatrix} A \\ B \end{pmatrix}_{z=l} = \hat{m}_I \begin{pmatrix} A \\ B \end{pmatrix}_{z=0}, \quad \hat{m}_I = \hat{K}(-\Phi+\tfrac{\gamma}{2})\hat{\mu}(s,\Phi)\hat{K}(-\tfrac{\gamma}{2}), \quad \Phi = Dl = (k-k_0)l, \quad \hat{\mu} = \begin{pmatrix} \alpha & \beta \\ \beta^* & \alpha^* \end{pmatrix}, \tag{12}$$
$$\alpha = \cosh G + i\Phi/G \sinh G, \quad \beta = is/G \sinh G, \quad G = \sqrt{s^2-\Phi^2}, \quad s = s_U = \pi n_1 l/\lambda_0 .$$

Subscript U points out relation to uniform gratings.

Having the propagation matrix $\hat{m}_I$ of a single VBG in an analytical form from Eq. (12) makes it possible to derive analytical expression of the bandwidth of a resonant cavity formed by two uniform VBGs with a mutual phase shift of π in their modulations. Matrix $\hat{m}_{II}$ of a second VBG attached at a distance l will have additional phase $\hat{K}$-matrix factors describing this longitudinal shift similar to Eq. (9). A π phase shift of the modulation of the second grating relative to the modulation of the first grating is equivalent to flipping the sign of n_1 and therefore s as well. The Lorentzian shape of the transmission peak can be written according to transmittance T from Eq. (6) similar to the last expression from Eq. (10) with the following intermediate derivation steps:

$$\begin{aligned} &\begin{pmatrix} A \\ B \end{pmatrix}_{z=2l} = \hat{m}_{II} \begin{pmatrix} A \\ B \end{pmatrix}_{z=l}, \qquad \hat{m}_{II} = \hat{K}(-kl)\hat{m}_I(-s,\Phi,\tfrac{Ql+\gamma}{2})\hat{K}(kl), \\ &\qquad\qquad \hat{M} = \hat{m}_{II}\hat{m}_I = \hat{K}(-2\Phi+\tfrac{\gamma}{2})\hat{\mu}(-s,\Phi)\hat{\mu}(s,\Phi)\hat{K}(-\tfrac{\gamma}{2}), \\ &M_{22} = e^{2i\Phi}(1 - is^{-1}\sinh(2s)\Phi - 2s^{-2}\sinh^2 s\Phi^2 + O(\Phi^3)), \\ &T = 1/\left|M_{22}\right|^2 \approx 1/(1+F_U\Phi^2), \quad F_U = 4s_U^{-2}\sinh^4 s_U . \end{aligned} \tag{13}$$

The last expression in Eq. (13) defines the bandwidth of a resonant cavity formed by two uniform π-shifted Bragg gratings of length l and reflection strength $s = s_U$ from Eq. (12) similar to the bandwidth from Eq. (11)

$$\Delta\lambda_{U,FWHM} = \lambda_0^2/(\pi n_0 l\sqrt{F_U}) = \lambda_0^2 s_U/(2\pi n_0 l \sinh^2 s_U) \tag{14}$$

Derivation of an analytical formula for the transmission peak bandwidth for the case of a moiré Bragg grating is more challenging because there is no analytical solution for the propagation matrix from Eq. (5) of the system of coupled wave equations in Eq. (3). In order to get the width of the peak approximated by the Lorentzian shape, we have to know the expansion of the propagation matrix element M_{22} up to the second power Φ according to Eq. (6). We will begin this derivation by rewriting the system of equations in Eq. (3) using notations from Eqs. (2),(8)-(10) as well as new notations such as ς for the dimensionless spatial variable

#212248 - $15.00 USD Received 16 May 2014; revised 25 Jul 2014; accepted 28 Jul 2014; published 15 Aug 2014

$$
\begin{aligned}
&z = \varsigma l/\pi, \quad \frac{d}{d\varsigma}\begin{pmatrix} A \\ B \end{pmatrix} = \tfrac{1}{2} s_{\mathrm{M}} \sin(\varsigma+\varphi)\begin{pmatrix} 0 & ie^{-2i\Phi\varsigma/\pi+i\gamma} \\ -ie^{2i\Phi\varsigma/\pi-i\gamma} & 0 \end{pmatrix}\begin{pmatrix} A \\ B \end{pmatrix}, \\
&0 \le \varsigma \le 2\pi, \\
&\begin{pmatrix} A \\ B \end{pmatrix} = \hat{K}\left(-\frac{\Phi}{\pi}\varsigma + \frac{\gamma}{2} + \frac{\pi}{4}\right)\begin{pmatrix} a \\ b \end{pmatrix} \quad \rightarrow \quad \frac{d}{d\varsigma}\begin{pmatrix} a \\ b \end{pmatrix} = \hat{w}(\varsigma)\begin{pmatrix} a \\ b \end{pmatrix}, \\
&\hat{w}(\varsigma) = \hat{w}_0(\varsigma) + i\Phi\hat{\sigma}, \quad \hat{w}_0(\varsigma) = \tfrac{1}{2} s_{\mathrm{M}} \sin(\varsigma+\varphi)\begin{pmatrix} 0 & 1 \\ 1 & 0 \end{pmatrix}, \quad \hat{\sigma} = \tfrac{1}{\pi}\begin{pmatrix} 1 & 0 \\ 0 & -1 \end{pmatrix}.
\end{aligned}
\tag{15}
$$

Here we performed the transition from wave amplitudes A and B to amplitudes a and b with phase K-matrix introduced in Eq. (9) and we get the coupling matrix with a linear dependence on detuning Φ. This allows the following iterative matrix derivations to be performed.

After substituting the solution for wave amplitudes a and b, in propagation matrix form, into the coupled wave equation, we get the differential equation of propagation matrix $\hat{m}(\varsigma)$ with identity condition at the boundary $\varsigma = 0$:

$$
\frac{d}{d\varsigma}\begin{pmatrix} a \\ b \end{pmatrix} = \hat{w}(\varsigma)\begin{pmatrix} a(\varsigma) \\ b(\varsigma) \end{pmatrix}, \quad \begin{pmatrix} a(\varsigma) \\ b(\varsigma) \end{pmatrix} = \hat{m}(\varsigma)\begin{pmatrix} a(0) \\ b(0) \end{pmatrix} \quad \rightarrow \quad \frac{d}{d\varsigma}\hat{m} = \hat{w}(\varsigma)\hat{m}(\varsigma), \quad \hat{m}(0) = \hat{1}. \tag{16}
$$

By representing the propagation matrix $\hat{m}(\varsigma)$ in the following expansion form with the detuning Φ, we get matrix equations with corresponding initial conditions from Eqs. (16),(15):

$$
\begin{aligned}
&\hat{m}(\varsigma) = \hat{m}_0(\varsigma)[\hat{1} + i\Phi\hat{u}^{(1)}(\varsigma) + (i\Phi)^2\hat{u}^{(2)}(\varsigma)]: \\
&\hat{m}(0) = \hat{1} \quad \rightarrow \quad \hat{m}_0(0) = \hat{1} = \hat{m}_0(2\pi), \quad \hat{u}^{(1,2)}(0) = 0; \\
&\tfrac{d}{d\varsigma}\hat{m} = \hat{w}\hat{m} \quad \rightarrow \quad \tfrac{d}{d\varsigma}\hat{m}_0 = \hat{w}_0\hat{m}_0, \quad \tfrac{d}{d\varsigma}\hat{u}^{(1)} = \hat{m}_0^{-1}\hat{\sigma}\hat{m}_0, \quad \tfrac{d}{d\varsigma}\hat{u}^{(2)} = \hat{m}_0^{-1}\hat{\sigma}\hat{m}_0\hat{u}^{(1)} = (\tfrac{d}{d\varsigma}\hat{u}^{(1)})\hat{u}^{(1)}.
\end{aligned}
\tag{17}
$$

Differential equations for matrices $\hat{m}_0$, $\hat{u}^{(1)}$ and $\hat{u}^{(2)}$ are relations at corresponding powers of detuning Φ in the differential equation for the whole matrix $\hat{m}$.

Propagation matrix $\hat{m}_0(\varsigma)$ at the exact Bragg condition, which is known from Eq. (7), allows the calculation of a first-order correction matrix $\hat{u}^{(1)}(2\pi)$ by integrating the corresponding differential equation in Eq. (17) over the whole moiré period

$$
\begin{aligned}
&\hat{m}_0(\varsigma) = \begin{pmatrix} \cosh S(\varsigma) & \sinh S(\varsigma) \\ \sinh S(\varsigma) & \cosh S(\varsigma) \end{pmatrix}, \quad S(\varsigma) = \tfrac{1}{2} s(\cos\varphi - \cos(\varsigma+\varphi)), \\
&\tfrac{d}{d\varsigma}\hat{u}^{(1)} = \hat{m}_0^{-1}\hat{\sigma}\hat{m}_0 = \tfrac{1}{\pi}\begin{pmatrix} \cosh(2S(\varsigma)) & \sinh(2S(\varsigma)) \\ -\sinh(2S(\varsigma)) & -\cosh(2S(\varsigma)) \end{pmatrix} \\
&\rightarrow \quad \hat{u}^{(1)}(2\pi) = 2I_0(s)\begin{pmatrix} \cosh(s\cos\varphi) & \sinh(s\cos\varphi) \\ -\sinh(s\cos\varphi) & -\cosh(s\cos\varphi) \end{pmatrix}.
\end{aligned}
\tag{18}
$$

Here $I_0(s) = J_0(is)$ is modified zero-order Bessel function.

After rewriting the last differential matrix equation in Eq. (17) in the form

$$
\tfrac{d}{d\varsigma}\hat{u}^{(2)} = \tfrac{1}{2}\tfrac{d}{d\varsigma}(\hat{u}^{(1)}\hat{u}^{(1)}) + \tfrac{1}{2}[(\tfrac{d}{d\varsigma}\hat{u}^{(1)})\hat{u}^{(1)} - \hat{u}^{(1)}(\tfrac{d}{d\varsigma}\hat{u}^{(1)})], \tag{19}
$$

one can check that the diagonal elements of the matrix expression in the square brackets are equal to zero. Finally, we get the propagation matrix element defining the bandwidth of a Lorentzian transmission peak:

#212248 - $15.00 USD Received 16 May 2014; revised 25 Jul 2014; accepted 28 Jul 2014; published 15 Aug 2014

$$u_{22}^{(2)}(2\pi)=\tfrac{1}{2}(\hat{u}^{(1)}(2\pi)\hat{u}^{(1)}(2\pi))_{22}=2I_0^2(s),$$
$$m_{22}(2\pi)=1-2iI_0(s)\cosh(s\cos\varphi)\Phi-2I_0^2(s)\Phi^2+iO(\Phi^3),\quad T=\frac{1}{|m_{22}|^2}=\frac{1}{1+F_{\rm M}\Phi^2+O(\Phi^4)},\tag{20}$$
$$F_{\rm M}=4I_0^2(s)\sinh^2(s\cos\varphi),\quad s=s_{\rm M},\quad \Delta\lambda_{\rm M,FWHM}=\frac{\lambda_0^2}{\pi n_0 l\sqrt{F_{\rm M}}}=\frac{\lambda_0^2}{2\pi n_0 l I_0(s_{\rm M})\sinh(s_{\rm M}\cos\varphi)}.$$

Here $s_{\rm M}$ is defined in Eq. (8).

We see that the bandwidth of the transmission peak in Eq. (20) is increasing with tuning of the envelope phase φ from zero. At $\varphi = \pi/2$ it actually has an infinite value. This means that the Lorentzian approximation for the shape of transmission peak is not valid anymore. To approximate the peak for this value of φ we need to take into account the next term which is proportional to the forth power of detuning Φ^4. We were able to find the expression for bandwidth of this double coherent moiré (DCM) filter formed by a cosine envelope profile corresponding to $\varphi = \pi/2$, though this derivation is rather cumbersome. The necessary calculation steps are presented in Appendix and the final result is

$$T=\frac{1}{1+H_{\rm M}\Phi^4},\quad H_{\rm M}^{1/2}=2I_0(s_{\rm M})L_0(s_{\rm M}),\quad \Delta\lambda_{\rm DCM,FWHM}=\frac{\lambda_0^2}{\pi n_0 l H_{\rm M}^{1/4}}=\frac{\lambda_0^2}{\pi n_0 l\sqrt{2I_0(s_{\rm M})L_0(s_{\rm M})}}.\tag{21}$$

Here the modified zero-order Bessel function $I_0(s)$ and the modified zero-order Struve function $L_0(s)$ with $s = s_{\rm M}$ from Eq. (8) have known power representations

$$I_0(s)=\sum_{k=0}^{\infty}s^{2k}/(2^k k!)^2,\quad L_0(s)=2/\pi\sum_{k=0}^{\infty}s^{2k+1}/[(2k+1)!!]^2.\tag{22}$$

For reference we would like to present analytical expressions for the bandwidths of transmission peaks in the case of double coherent cavities formed by thin reflective elements and by uniform Bragg gratings. A double coherent reflector (DCR) cavity formed by consecutive thin reflectors with strengths ½*s*, –*s* and ½*s* separated by *l* has a bandwidth of the 100% resonant transmission peak given by:

$$T=1/(1+H_{\rm R}\sin^4\Phi),\quad H_{\rm R}=\sinh^2(2s),\quad \Delta\lambda_{\rm DCR,FWHM}=\lambda_0^2/(\pi n_0 l H_{\rm R}^{1/4}),\tag{23}$$

This result can be derived in terms of the transfer matrix approach used in Eqs. (9),(10).

Double coherent resonant cavity formed by three Bragg gratings of lengths ½*l*, *l* and ½*l* with the same amplitude of modulation n_1 and mutual π-shifts should demonstrate a flat-top 100% transmission peak occurring at resonant Bragg wavelength λ_0 with a bandwidth derived in a fashion similar to Eq. (13)

$$\hat{m}=\hat{\mu}(\tfrac{s}{2},\tfrac{\Phi}{2})\hat{\mu}(-s,\Phi)\hat{\mu}(\tfrac{s}{2},\tfrac{\Phi}{2}),\quad T=|m_{22}|^{-2}=1/(1+H_{\rm U}\Phi^4),$$
$$H_{\rm U}=4s^{-4}(\cosh s-1)^2\sinh^2 s,\quad \Delta\lambda_{\rm DCU,FWHM}=\lambda_0^2/(\pi n_0 l H_{\rm U}^{1/4}),\tag{24}$$

where reflection strength *s* is equal $s_{\rm U}$ from Eq. (12).

5. Physical implementation

In order to verify the theoretically predicted bandwidths and peak shapes for a moiré VBG filter of varying φ values a moiré VBG similar to the one in Fig. 1(a) was created. This moiré VBG was designed to demonstrate the concept of a filter with tunable bandwidth by transverse change of the position of incidence. Measurement of the spectral transmission at varying transverse locations along the grating allowed us to prove the validity of the obtained formulae in Eq. (20) and Eq. (21).

To create the moiré VBG for testing, a PTR glass specimen was sequentially exposed to two UV interference patterns designed to individually create two reflective VBGs with slightly different resonant wavelengths close to $\lambda_0 = 1.064$ μm. The superposition of these two

#212248 - $15.00 USD Received 16 May 2014; revised 25 Jul 2014; accepted 28 Jul 2014; published 15 Aug 2014

gratings generated the moiré pattern discussed in Eq. (1). Then the specimen was thermally developed to produce permanent RIM of the moiré pattern. The semi-period of the slowly varying envelope was determined from side illuminating the specimen in a transmission VBG regime with longitudinal translation along z-direction. It was observed that the efficiency of the diffraction in the transmission regime had a periodicity of $l = ½L = 1.635$ mm relating to the semi-period of the moiré pattern in the reflection regime.

The background refractive index of the PTR glass is $n_0 = 1.485$ at λ_0. The amplitude of RIM for each grating was estimated to be $n_1 = 215$ ppm based on the technical parameters of recording and development procedure. Thus, the maximum amplitude of the moiré envelope is $N_1 = 2n_1 = 430$ ppm from Eq. (2) and the reflection strength of one semi-period is $s_M = 2N_1 l/\lambda_0 = 1.32$ from Eq. (8).

In the device under consideration, both recorded Bragg wave vectors $\mathbf{Q}_1$ and $\mathbf{Q}_2$ are collinear along the z-axis. Two parallel cuts of this specimen with separation $L = 2l = 3.27$ mm were made at a small angle $\theta \approx 5° = 0.087$ rad with respect to the Bragg modulation fringe planes. This small angle is used to provide transverse variation of the moiré envelop similar to that illustrated on Fig. 1(a). The magnitude of the transverse shift along x-direction necessary to change the envelope profile from a sine period to a cosine period is about $½l/\theta = 9.4$ mm. In order for laser beam propagation inside the moiré VBG to be normal to the fringe planes, the VBG should be placed at a small angle $n_0\theta$ in air with respect to the incident beam. This skew incidence leads to a trivially small constant transverse shift of the transmitted beam due to refraction on parallel surfaces of the glass specimen. The more advanced situation proposed in Fig. 1(a) where vectors $\mathbf{Q}_1$ and $\mathbf{Q}_2$ were not exactly collinear but had a small specific mutual angle is able to provide a device where light is incident along the surface normal. This ability to vary the directions of the recorded grating wave vectors inside the multiplexed VBG would give more opportunities for the design of sophisticated resonant optical elements for different laser applications [18].

Measurements of the transmission spectrum at different transverse points along the moiré VBG were performed using a tunable laser source with beam diameter of 1 mm. The small beam diameter was used so that the effect of inhomogeneity in the grating properties across the beam aperture would be minimized. Also with larger beam sizes the aperture of the beam would encircle areas of the tilted grating with phase φ in significant range to produce some convolution of spectrum across the beam aperture such as described in [19] and a small beam minimizes these effects. The tunable laser was incident normal to the fringe planes of the grating structure and, as the wavelength of the incident beam was swept through its range, the transmitted power through the moiré VBG was monitored. Figure 2 shows experimental and numerical data for cases where light is incident on a moiré envelope with a sine and a cosine profile.

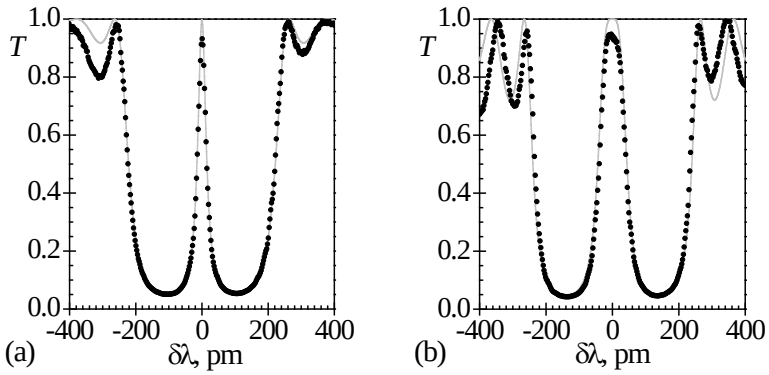

Fig. 2. Experimental (dots) and numerically modeled (line) irradiance transmission versus spectral detuning $\delta\lambda = \lambda - \lambda_0$: (a) sine moiré envelope profile; (b) cosine profile.

#212248 - $15.00 USD Received 16 May 2014; revised 25 Jul 2014; accepted 28 Jul 2014; published 15 Aug 2014

We see that experimental spectra are fit with good accuracy by numerical solutions of the coupled wave system in Eq. (3) with the characteristic parameters of this moiré VBG discussed above.

6. Discussion of experimental results

Figure 3 shows actual bandwidths of the moiré VBG measured at different transverse illumination positions with steps of 1 mm along the transverse *x*-axis, see Fig. 1(a). The *x*-coordinate has been recalculated in terms of the initial phase φ of the envelope profile $n_{1,\varphi}(z)$ in Eq. (2). The solid line from numerical modeling of Eq. (3) fits well with the dots representing the experimental data. The range of FWHM bandwidths along this device aperture ranges from 30 pm to 90 pm. Deviation of experimental dots from simulation curve is due to both measurement errors and inhomogeneities of fabricated moiré VBG filter. The dashed line on Fig. 3 is our simple analytical result from Eq. (20) for a Lorentzian peak bandwidth which gives very good approximation for envelope angles $0 \le \varphi \le \pi/4$. The square symbol with a horizontal dotted line on Fig. 3 is an analytical result from Eq. (21) for the flat-top peak bandwidth in the case of a cosine envelope profile with $\varphi = ½\pi$. The dashed and dotted lines provide good estimates for the tunable bandwidth of our one moiré envelope period VBG with arbitrary phase φ defining any possible envelope profile between the two extreme cases of sine and cosine profiles.

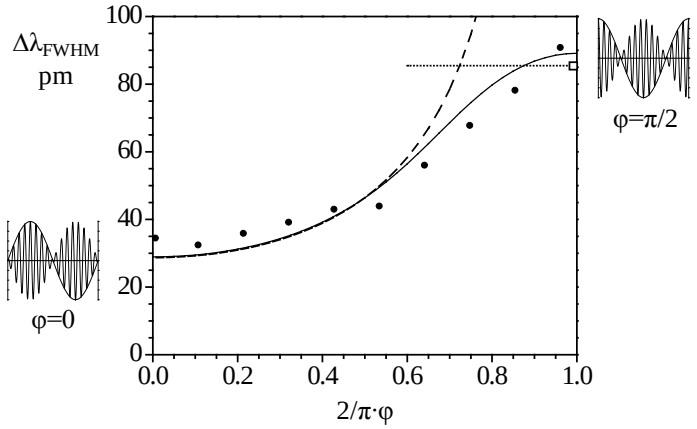

Fig. 3. FWHM bandwidth of moiré VBG versus the tunable envelope phase parameter $2\varphi/\pi$: dots – experimental measurements, solid line – numerical modeling, dashed line – analytical expression (20) for the bandwidth of a Lorentzian peak, square dot with dotted line – analytical expression (21) for the bandwidth of a flat-top peak of a double coherent resonant cavity.

The analytical result in Eq. (21) describing the transmission peak using only the forth power of detuning Φ^4 gives an approximation error of 4.1% in comparison with the numerical simulations for a moiré reflection strength of $s_M = 1.32$, see solid and dotted lines at the right edge of Fig. 3. With an increasing s_M, the approximation accuracy for the FWHM bandwidth of the flat-top transmission peak for the double coherent resonant cavity of a moiré cosine envelope profile improves and for $s_M = 2$, the approximation error is reduced to 1.2%. The ratio of maximum to minimum bandwidth also depends on the moiré reflection strength; in our case it is approximately 3.1 for $s_M = 1.32$ and it is 5.6 for $s_M = 2$.

All of the measured spectra for the envelope profiles with different phase φ have demonstrated resonant peak transmissions of 95% or more using the previously mentioned 1 mm diameter beam. The decrease of a resonant transmission from 100% can be due to fabrication non-uniformities in the VBG causing small spectral shifts of the transmission peak position for different aperture points. As a result, each of the total transmission spectra after integrating over the whole beam cross-section will demonstrate slightly washed out transmission peak producing reduced maximum transmission value. Another important cause

#212248 - $15.00 USD Received 16 May 2014; revised 25 Jul 2014; accepted 28 Jul 2014; published 15 Aug 2014

of reduced resonant transmittance is optical loss in glass, mostly due to scattering. The decimal loss coefficient in PTR glass of the studied grating is $\alpha_{10} = 0.005$ cm^{-1}, and it can be as low as 0.001 cm^{-1} for PTR glass [16]. This parameter describes a decrease of the wave intensity with propagation as $\propto 10^{-\alpha_{10} z} = e^{-\alpha z}$, so the natural loss coefficient is $\alpha = \alpha_{10}\ln 10 = 2.3\alpha_{10}$ and wave amplitude decreases as $\propto \exp(-\frac{1}{2}\alpha z)$.

We can estimate the decrease of the resonant transmission peak from coupled wave system in Eq. (15) at exact resonance without a detuning matrix term $i\Phi\hat{\sigma}$ in $\hat{w}(\varsigma)$, but with amplitude loss matrix term $-\frac{1}{2}\alpha l\hat{\sigma}$ for counter-propagating waves. The determinant of the propagation matrix $\hat{m}$ still equals one which follows mathematically from the condition $\mathrm{tr}(\hat{w}) = 0$ valid in our current case of counter-propagating waves experiencing the same longitudinal losses. As a result, the equation for the amplitude transmission coefficient in Eq. (6) is still correct. Finally, with the use of correction matrix term $\hat{u}^{(1)}(2\pi)$ from Eq. (18) we obtain the following first-order correction to the resonant transmission peak of a moiré filter with tunable bandwidth

$$\hat{m}(2\pi) = \hat{1} - \tfrac{1}{2}\alpha l\hat{u}^{(1)}(2\pi) + O(\alpha^2), \quad T = 1/m_{22}^2 \approx 1 - 2I_0(s_{\mathrm{M}})\cosh(s_{\mathrm{M}}\cos\varphi)\alpha l. \tag{25}$$

Using the values $\alpha = 2.3\alpha_{10} = 0.0115$ cm^{-1}, $s_{\mathrm{M}} = 1.32$ and $l = 1.635$mm from the actual fabricated moiré VBG and Eq. (25), we expect a theoretical value $T = 98.9\%$ for the reduced resonant transmission in the case of the sine envelope profile with $\varphi = 0$, which is most sensitive to losses due to its producing the narrowest transmission peak. So, there are possibilities for increasing the experimental value of 95% for transmission by improving the parameters of the recording process. Still, for recording resonant Bragg filters with much more narrow intended bandwidth, the losses could be one of the main limiting factors for the maximum resonant transmission.

7. Conclusion

The moiré VBG filter with tunable bandwidth is suggested as an optical element for laser design and for significant narrowing of emission spectra of lasers of different types. Detailed theoretical analysis based on transfer matrix approach with an additional expansion of the propagation matrix in a power series of spectral detuning was used to derive analytic expressions for the tunable bandwidth of a moiré VBG filter. This analysis provided expressions for both the Lorentzian transmission peak of a one-period sine moiré cavity and for the flat-top transmission peak generated by a double coherent resonant cavity occurring in the case of a one-period cosine moiré envelope profile. An analytic expression was also derived for the reduction of the resonant peak transmission due to losses that can exist in actual devices. A robust monolithic large-aperture moiré VBG filter was fabricated in a material known to be tolerant to high-power laser irradiation. The processing of this device enabled creating a filter with a tunable spectral bandwidth at a fixed resonant wavelength which confirmed our theoretical results.

Appendix

Let us calculate the parameter H in Eq. (21). In the case of a cosine envelope profile with phase $\varphi = \frac{1}{2}\pi$, the integral strength along the grating is $S(\varsigma) = \frac{1}{2}\sin\varsigma$ according to Eq. (18). By expanding the matrix $\hat{m}(\varsigma)$ up to the forth power of Φ and using differential equations for $\hat{u}^{(3)}(\varsigma)$ and $\hat{u}^{(4)}(\varsigma)$, similar to the ones in Eq. (17), one can show that

$$\hat{m}(2\pi) = \begin{pmatrix} m_{22}^* & m_{12} \\ m_{12} & m_{22} \end{pmatrix}, \quad \begin{matrix} m_{12} = 1 - \Phi^2 U_{12}^{(2)} + \Phi^4 U_{12}^{(4)}, \quad U_{pq}^{(j)} = u_{pq}^{(j)}(2\pi), \\ m_{22} = 1 - 2iI_0(s)\Phi - 2I_0^2(s)\Phi^2 - i\Phi^3 U_{22}^{(3)} + \Phi^4 U_{22}^{(4)}, \end{matrix} \tag{26}$$

$$U_{12}^{(2)} = \tfrac{1}{\pi^2}\int_0^{2\pi} d\xi \int_0^{\xi} d\eta \sinh(s(\sin\eta - \sin\xi)) = 2I_0(s)L_0(s).$$

#212248 - $15.00 USD Received 16 May 2014; revised 25 Jul 2014; accepted 28 Jul 2014; published 15 Aug 2014

Here matrix element $U_{12}^{(2)}$ has been calculated analytically and it is equal to twice the product of a modified zero-order Bessel function $I_0(s)$ and a modified zero-order Struve function $L_0(s)$.

The square of the absolute value of the matrix element defining the transmission spectrum according to Eqs. (6),(21),(26) is

$$\left|m_{22}\right|^2 = 1 + H\Phi^4 + ..., \quad H = 4I_0^4(s) - 4I_0(s)U_{22}^{(3)} + 2U_{22}^{(4)}. \tag{27}$$

From the other side, the determinant of the propagation matrix is equal one and it does not depend on spectral detuning. So all coefficients at powers of Φ in the calculated determinant of the matrix expansion from Eq. (26) should be equal to zero

$$\det \hat{m} = 1 + \underbrace{[4I_0^4(s) - 4I_0(s)U_{22}^{(3)} + 2U_{22}^{(4)} - (U_{12}^{(2)})^2]}_{=0}\Phi^4 + ... = 1, \tag{28}$$

Comparing Eq. (27) and Eq. (28) we get with Eq. (26)

$$\left|m_{22}\right|^2 = 1 + H\Phi^4, \quad H = (U_{12}^{(2)})^2, \quad U_{12}^{(2)} = 2I_0(s)L_0(s). \tag{29}$$

We have used this expression in Eq. (21).

Acknowledgments

The work was partially supported by HEL JTO, contract W911NF-10-1-0441.

#212248 - $15.00 USD Received 16 May 2014; revised 25 Jul 2014; accepted 28 Jul 2014; published 15 Aug 2014